AGATA at GSI-FRS
MC-Simulations

C. Domingo-Pardo, J. Gerl, H.J. Wollersheim

November 19, 2010

1 Introduction

This report presents a summary on the expected peformance of AGATA for experiments at the GSI fragment separator FRS. The main focus are the attainable efficiency and resolution values. Only shell AGATA geometries have been considered, although with a variable number of double- and triple-cluster detectors. This should allow one to pick-up expected efficiency and resolution values according to the number of crystals available for the array at the time of experiment. An overview on the general experimental setup is given in Sec. 2. The MC-simulated performance for a representative physics case if described in Sec. 3. Here, almost all possible combinations of double- and triple-cluster detectors, from 10 up to 40 capsules are displayed and tabulated. Efficiency and resolution results are represented as a function of the distance target-array, which can be adjusted for each particular experiment in order to find the best compromise between efficiency and resolution. In these results a simplified add-back algorithm is generally used for the γ-ray energy reconstruction. A comparison versus a realistic tracking algorithm is given in Sec. 4. The effect of a 2 mm lead absorber in the efficiency, which is -in principle- foreseen to reduce the low energy background rate is presented in Sec. 5. The dependence of the efficiency with the angle θ_γ is displayed in Sec. 6. The dependence of efficiency and resolution on the gamma-energy is reported in Sec. 7 for γ-rays in the energy range from 500 keV up to 4 MeV and for several AGATA configurations. An example of lifetime measurement via the line-shape effect or Doppler-Shift Attenuation Method is shown in Sec. 8.

2 The GSI fragmentation facility and the spectroscopy area

In-beam γ-ray spectroscopy experiments start with a very intense primary beam of a stable isotope, delivered by the SIS synchrotron. This primary beam impinges at a very high energy,

typically between 500 MeV/u and 1 GeV/u on a production target. The latter is in most cases a Be- or a Pb-layer with a thickness of 2-4 g/cm^2. The fragment of interest is selected and transmitted through the fragment separator (FRS) using the Bρ-ΔE-Bρ method. Details on the FRS can be found in Ref. [1]. The spatial profile of the fragmented beam at the final focal plane of the FRS typically shows a width of 6 cm FWHM in the dispersive plane X and about 4 cm FWHM on the vertical axis Y (see Fig. 1).

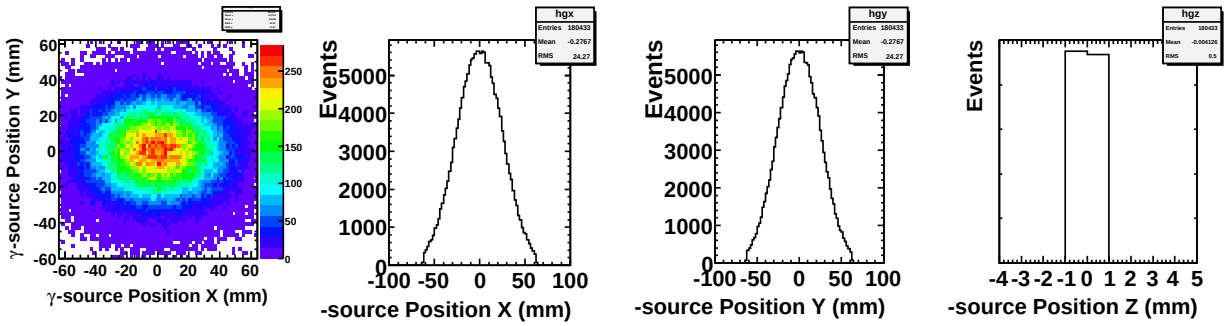

Figure 1: Beam profile at the FRS focal plane.

A secondary target is placed at this final focal plane of the FRS. The target material is usually gold for Coulomb excitation or beryllium for secondary fragmentation or particle knockout reactions. Thanks to the very high secondary beam energy of typically $\sim$100 MeV/u, rather thick targets of 200 mg/cm^2 to 500 mg/cm^2 can be used, which allow one to keep the angular straggling of the recoil nuclei within reasonable limits of 5-10 mrad. As it is shown below, other target materials as e.g. Iron may be preferred and used for lifetime measurements via the Doppler-Shift Attenuation Method (DSAM). Attached to the secondary target is a double-sided silicon-strip detector (DSSD) which serves to determine the position of the recoil fragments. The latter, in combination with the 3D-spatial sensitivity of AGATA and the Lund-York-Cologne Calorimeter (LYCCA) is used to determine accurately the Doppler-Correction on an event-by-event basis. Details about γ-ray spectroscopy experiments with RIB at the FRS can be found in Ref. [2].

3 Reference case and AGATA performance

A representative -simplified- physics case has been simulated in order to study the attainable γ-ray detection efficiency and resolution for experiments at FRS. The MC-code is the one from Ref. [3] with very little modifications in order to include the specific beam spatial-profile of the FRS. Several scenarios have been considered in order to account for the availability of double and triple cluster detectors by the time of the experiment. This reference case is

based on 1×10^5 MC-histories corresponding to γ-rays with an energy at rest of $E_{\gamma,\circ}$ =1 MeV emitted from a nucleus at a recoil velocity of β =0.43, equivalent to 100 MeV/u commonly used for Coulomb excitation and fragmentation experiments at GSI. In all cases a γ-ray multiplicity of M_γ=1 has been assumed. In this simulation work, the event reconstruction algorithm used to recover the original γ-ray energy is a simplified add-back method between all the segments in the shell, applicable only to simulated data. In this respect, the values quoted below have to be rather considered as upper limits. For the Doppler-correction, the γ-ray hit with largest deposited energy within one event was assumed to be the first interaction, which was used to provide the incident γ-ray direction. A position resolution of 5 mm FWHM has been included in the spatial uncertainty.

Table 4 shows the expected performance in terms of γ-ray efficiency and resolution as a function of the number of triple and double cluster detectors available and for several distances from the secondary target to the shell-array. A spherical target chamber is foreseen, which will allow one to shift the position of the secondary target along the beam axis z. Such dynamic range allows one to find the best compromise in terms of efficiency and resolution according to the needs of each particular experiment. This is illustrated in Fig. 2, where two different target-array distances are shown. The structural materials in the simulation include the aluminium endcap of the cluster detectors, a beam-pipe of 120 mm diameter and 4 mm thick aluminium, and an aluminium target chamber of 23 cm radius and 4 mm thickness. The γ-ray events have been simulated with the spatial profile of the ion beam, and with a constant emission profile along a 500 mg/cm^2 thick iron target.

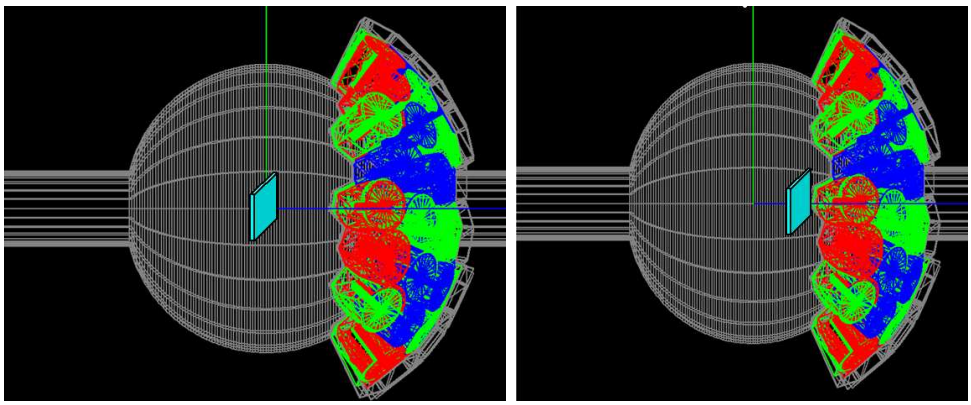

Figure 2: Schematic view of the AGATA setup comprising 10 triple and 5 double cluster detectors. Two possible positions of the secondary target are shown.

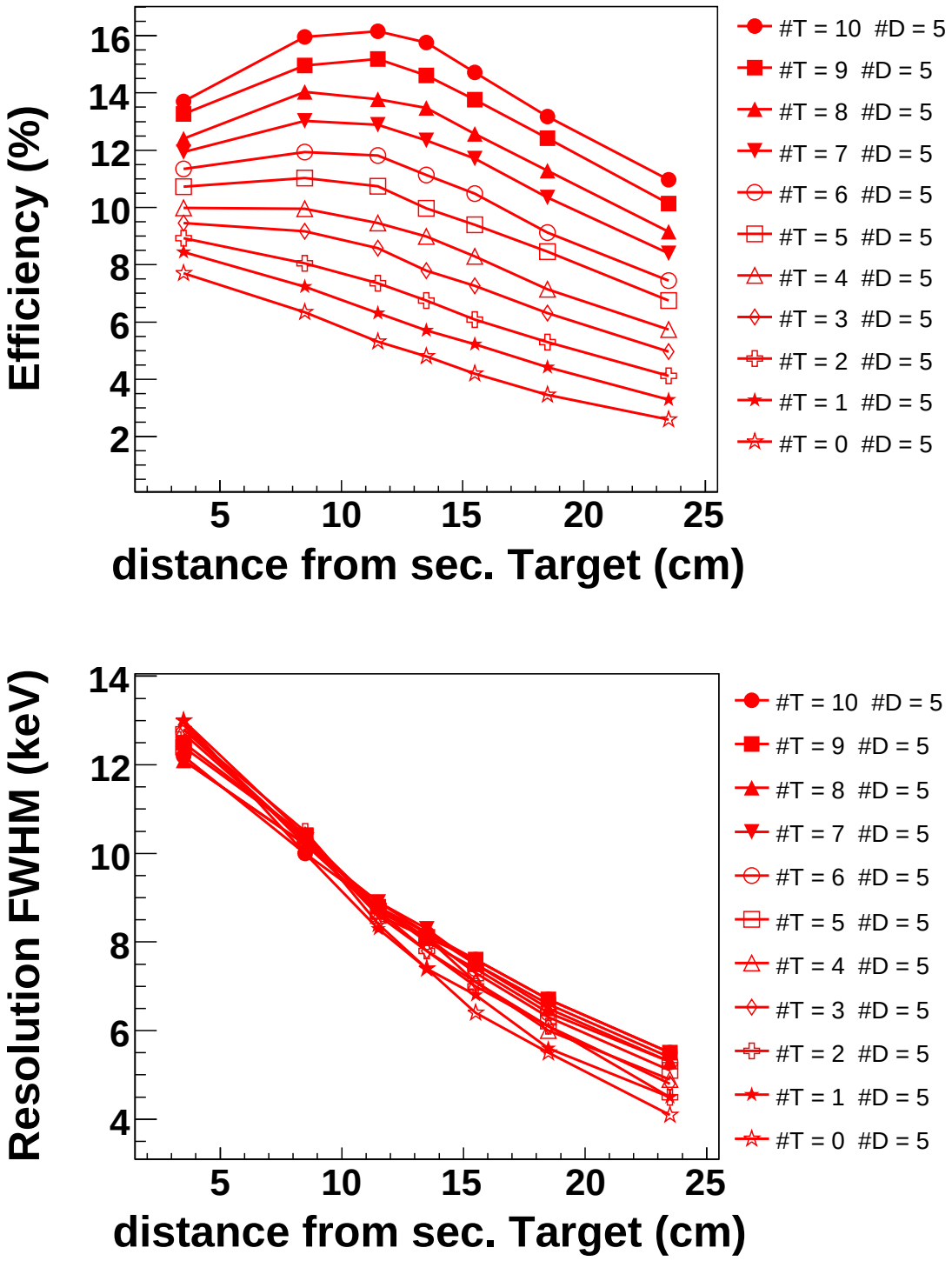

Figure 3: Efficiency (top) and resolution (bottom) as a function of the number of triple (#T) cluster detectors in the setup. The number of double cluster detectors is always 5.

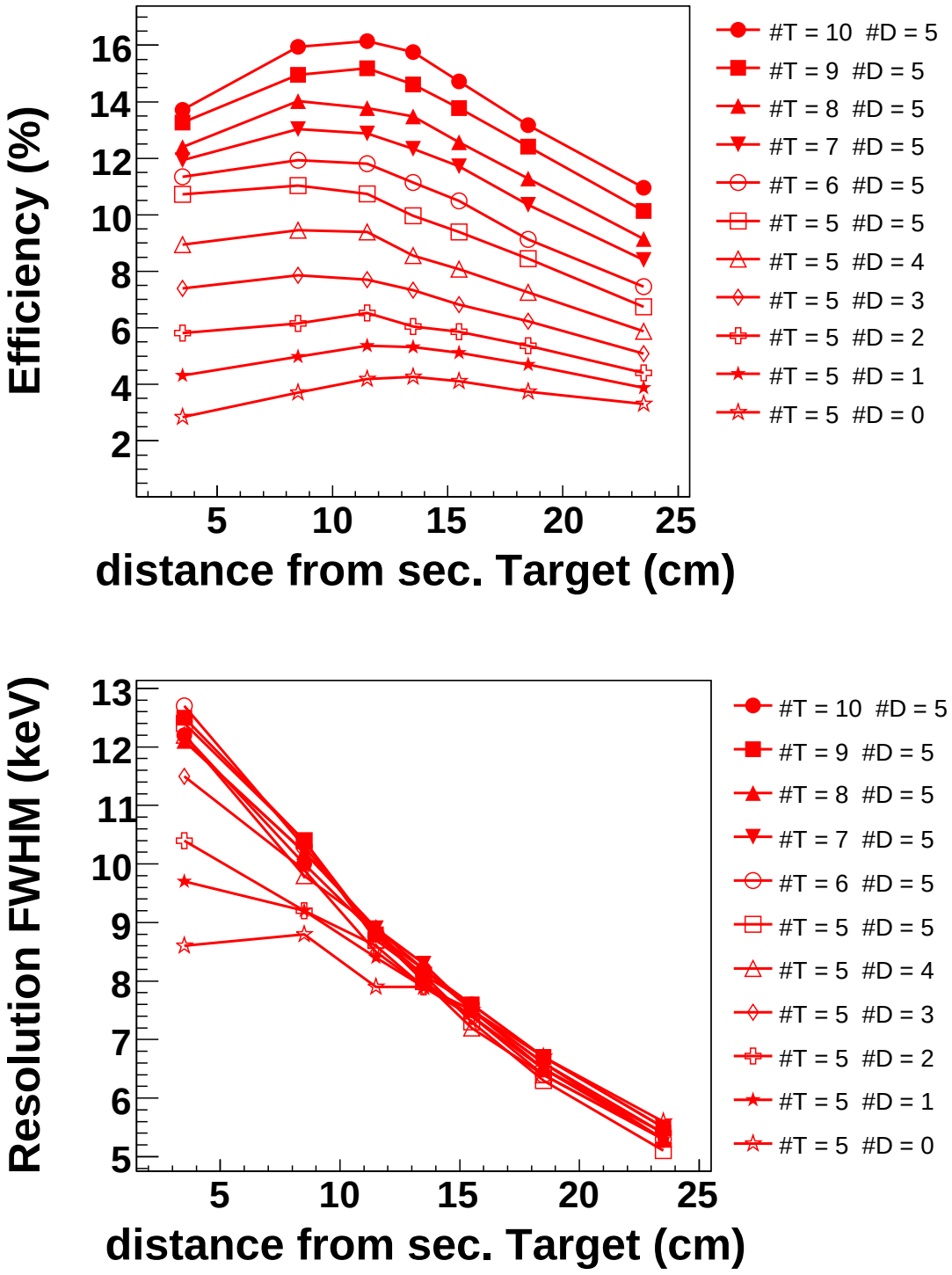

Figure 4: Efficiency (top) and resolution (bottom) as a function of the number of triple (#T) and double (#D) AGATA cluster detectors in the setup.

Table 1: Efficiency and resolution values as a function of the number of double and triple AGATA cluster detectors available. For each configuration, the first raw are the efficiency values and the second raw the resolution in FWHM.

Nr. of	Nr. of	distance target-array (cm)							
triple	double	23.5	18.5	15.5	13.5	11.5	8.5	3.5	
10	5	11.0	13.2	14.7	15.8	16.1	15.9	13.7	(%)
		5.5	6.7	7.6	8.2	8.8	10.0	12.2	(keV)
9	5	10.1	12.4	13.8	14.6	15.2	15.0	13.3	(%)
		5.5	6.7	7.6	8.1	8.8	10.4	12.5	(keV)
8	5	9.1	11.3	12.6	13.5	13.8	14.0	12.4	(%)
		5.3	6.5	7.5	8.2	8.9	10.2	12.1	(keV)
7	5	8.4	10.4	11.7	12.3	12.9	13.0	11.9	(%)
		5.4	6.6	7.5	8.3	8.9	10.2	12.1	(keV)
6	5	7.4	9.1	10.5	11.1	11.8	11.9	11.3	(%)
		5.3	6.4	7.4	8.0	8.8	10.3	12.7	(keV)
5	5	6.8	8.4	9.4	10.0	10.7	11.0	10.7	(%)
		5.1	6.3	7.3	8.1	8.7	10.4	12.4	(keV)
4	5	5.7	7.1	8.3	9.0	9.4	9.9	10.0	(%)
		4.9	6.0	7.1	8.1	8.6	10.3	12.8	(keV)
3	5	5.0	6.3	7.3	7.8	8.6	9.2	9.4	(%)
		4.8	6.1	7.1	7.8	8.7	10.2	12.9	(keV)
2	5	4.1	5.3	6.1	6.8	7.4	8.1	8.9	(%)
		4.5	6.1	7.0	7.8	8.6	10.5	12.8	(keV)
1	5	3.3	4.4	5.2	5.7	6.3	7.2	8.4	(%)
		4.5	5.6	6.8	7.4	8.3	10.0	13.0	(keV)
0	5	2.6	3.5	4.2	4.8	5.3	6.3	7.7	(%)
		4.1	5.5	6.4	7.4	8.4	10.4	13.0	(keV)
5	4	5.9	7.2	8.1	8.6	9.4	9.4	8.9	(%)
		5.3	6.4	7.2	8.0	8.9	9.8	12.2	(keV)
5	3	5.1	6.2	6.8	7.3	7.7	7.9	7.4	(%)
		5.3	6.5	7.4	7.9	8.5	9.9	11.5	(keV)
5	2	4.4	5.4	5.9	6.1	6.5	6.2	5.8	(%)
		5.4	6.5	7.4	7.9	8.6	9.2	10.4	(keV)
5	1	3.9	4.7	5.1	5.3	5.4	5.0	4.3	(%)
		5.3	6.6	7.5	7.9	8.4	9.2	9.7	(keV)
5	0	3.3	3.7	4.1	4.3	4.2	3.7	2.8	(%)
		5.6	6.7	7.5	7.9	7.9	8.8	8.6	(keV)

4 Effect of the γ-ray tracking algorithm

The simplified add-back method implemented in the reconstruction algorithm after the simulation in order to recover the incident γ-ray energy is compared in Fig. 5 versus a realistic tracking algorithm (MGT [4]). The results are in general very similar, only substantial discrepancies are found for the case of 5 double cluster detectors ring, but one has to consider that the MGT-code was used in a "default" mode, and no attempt was made to optimize the results. With some improvements, most probably the differences will be smaller.

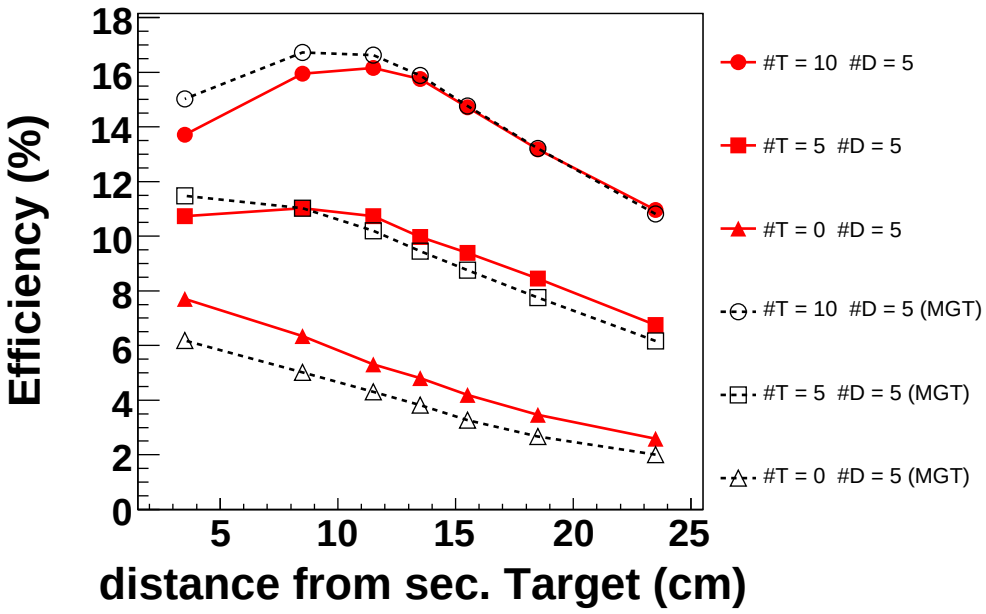

Figure 5: Solid symbols represent the efficiency calculated by means of a simplified/idealistic add-back algorithm (applicable only to simulated data), the open symbols show the efficiency obtained with the MGT code (standard-mode, not fully optimized).

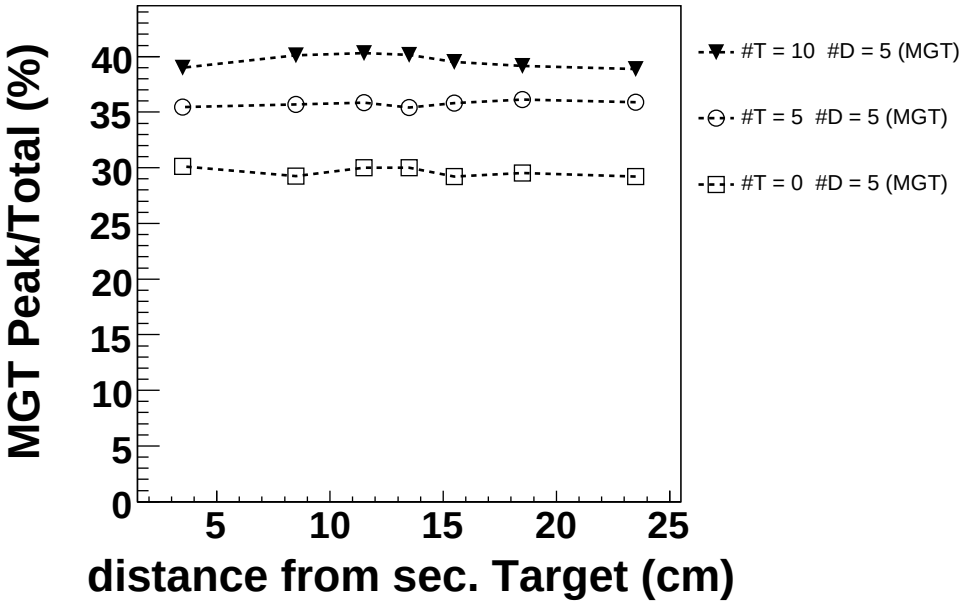

Figure 6: Peak-to-total ratios obtained with the MGT-code (standard-mode, not fully optmized).

5 Impact of lead absorber

Fig. 7 shows the effect of a 2 mm Lead layer around the target chamber, which is foreseen in order to shield the AGATA clusters from the low energy bremsstrahlungs-radiation. Three configurations have been considered in the simulation, *i*) 10 triple + 5 double, *ii*) 5 triple + 5 double and *iii*) 5 double cluster detectors. The impact of this lead layer seems to be lower for the double-cluster detectors and for the nominal distance (23.5 cm) due to the larger Doppler-shifted energies at the subtended angles. The resolution remains the same.

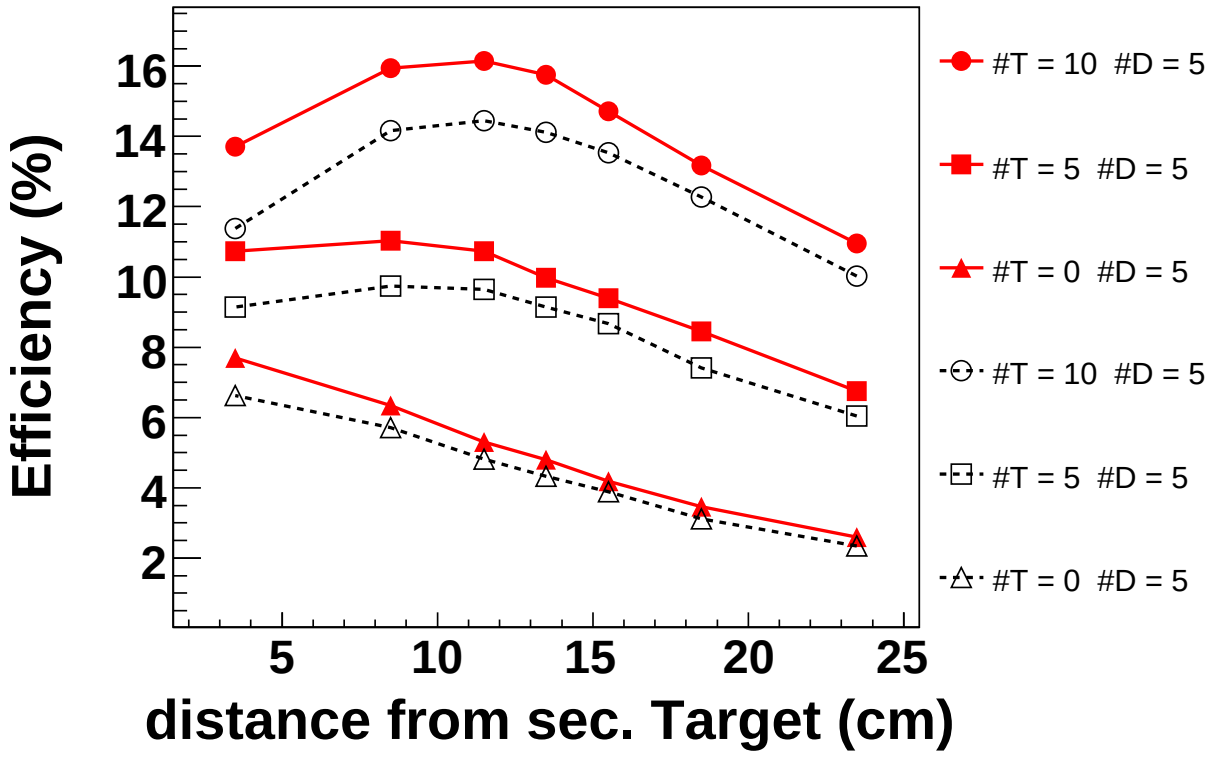

Figure 7: Solid symbols represent the original efficiency without lead absorber, the empty symbols show the deterioration of the efficiency due to a 2 mm thick lead absorber infront of the detectors.

6 Angular distribution of the efficiency

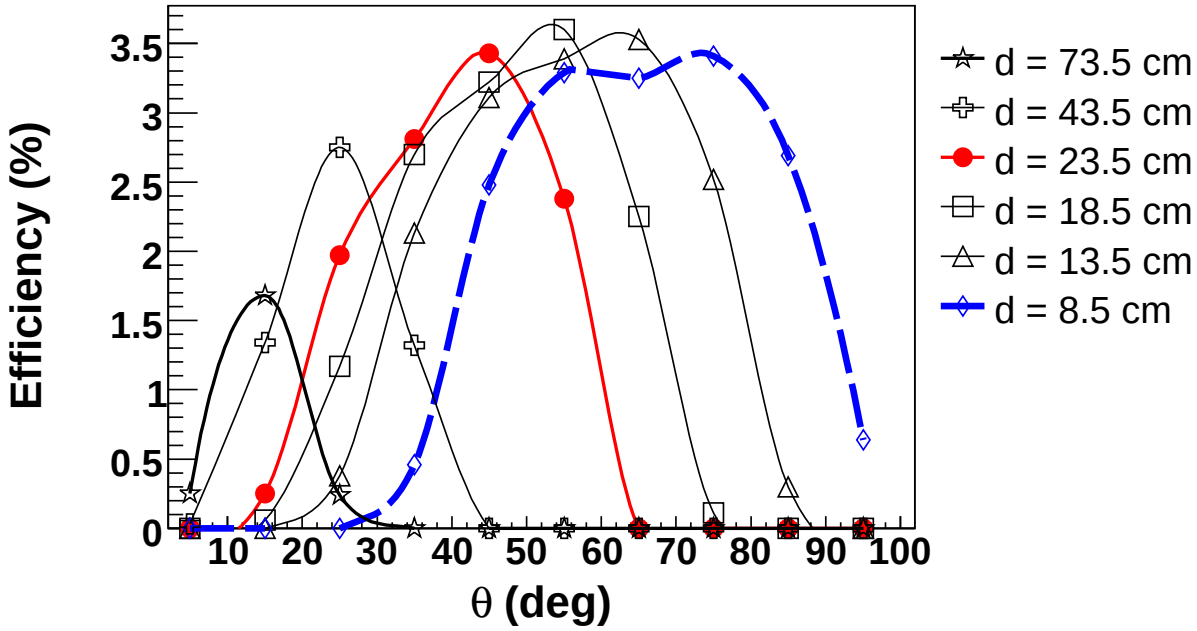

Figure 8: Efficiency as a function of the γ-ray detection angle θ_γ. The simulation comprises 10 triple and 5 double AGATA cluster detectors.

7 Energy dependence of efficiency and resolution

7.1 10 triple + 5 double

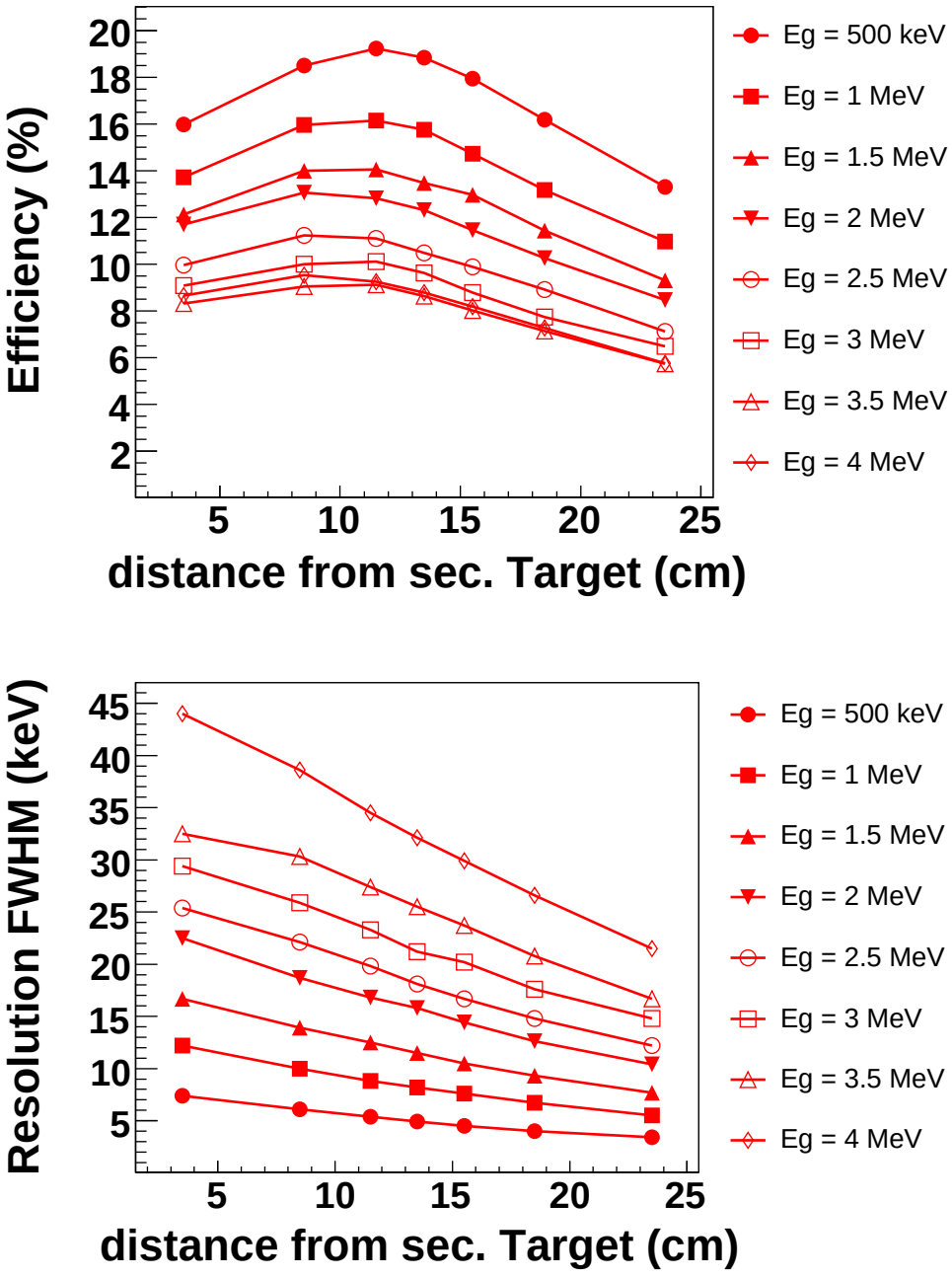

Figure 9: Photopeak efficiency (top) and resolution (bottom) for 10 triple + 5 double AGATA cluster detectors. Each curve corresponds to one gamma-ray energy (see figure label).

Table 2: 10 triple + 5 double AGATA configuration, efficiency and resolution values as a function of the γ-ray energy at rest $E_{\gamma,\circ}$ and $\beta = 0.43$. For each configuration, the first raw are the efficiency values and the second raw the resolution in FWHM.

$E_{\gamma,\circ}$	distance target-array (cm)							
(keV)	23.5	18.5	15.5	13.5	11.5	8.5	3.5	
500 keV	13.3	16.2	17.9	18.8	19.2	18.5	16.0	(%)
	3.4	4.0	4.5	4.9	5.4	6.1	7.4	(keV)
1 MeV	11.0	13.2	14.7	15.8	16.1	15.9	13.7	(%)
	5.5	6.7	7.6	8.2	8.8	10.0	12.2	(keV)
1.5 MeV	9.3	11.4	13.0	13.5	14.1	14.0	12.1	(%)
	7.7	9.3	10.5	11.5	12.5	13.9	16.7	(keV)
2 MeV	8.5	10.2	11.4	12.3	12.8	13.1	11.7	(%)
	10.4	12.6	14.4	15.8	16.8	18.7	22.5	(keV)
2.5 MeV	7.1	8.9	9.9	10.5	11.1	11.2	10.0	(%)
	12.2	14.8	16.7	18.1	19.8	22.1	25.4	(keV)
3 MeV	6.5	7.7	8.8	9.6	10.1	10.0	9.1	(%)
	14.8	17.6	20.2	21.2	23.3	25.9	29.4	(keV)
3.5 MeV	5.7	7.1	8.0	8.6	9.1	9.1	8.3	(%)
	16.7	20.8	23.7	25.5	27.4	30.3	32.5	(keV)
4 MeV	5.8	7.3	8.2	8.8	9.2	9.5	8.6	(%)
	21.5	26.6	29.9	32.1	34.5	38.6	44.0	(keV)

7.2 5 triple + 5 double

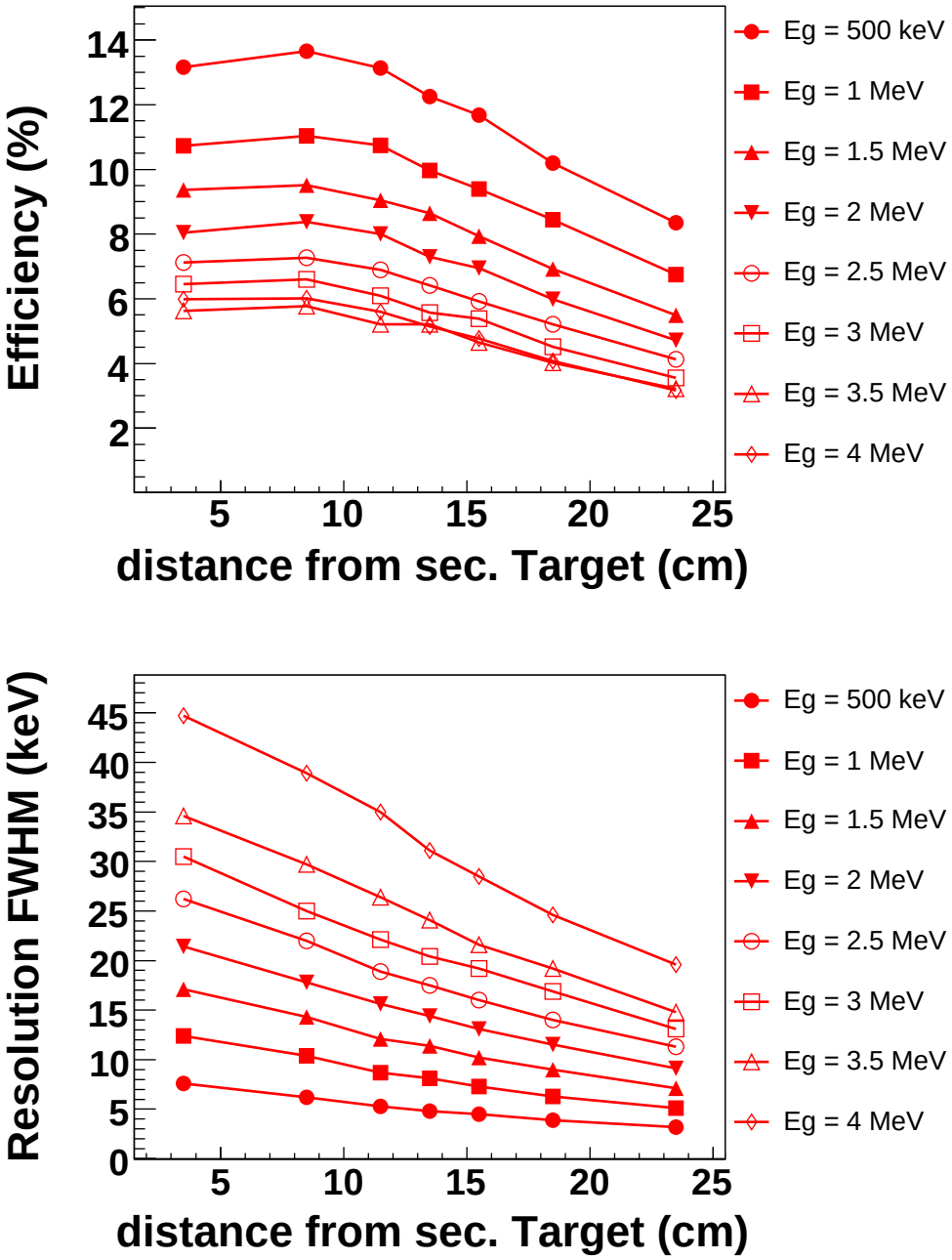

Figure 10: Photopeak efficiency (top) and resolution (bottom) for 5 triple + 5 double AGATA cluster detectors. Each curve corresponds to one gamma-ray energy (see figure label).

Table 3: 5 triple + 5 double AGATA configuration, efficiency and resolution values as a function of the γ-ray energy at rest $E_{\gamma,\circ}$ and $\beta = 0.43$. For each configuration, the first raw are the efficiency values and the second raw the resolution in FWHM.

$E_{\gamma,\circ}$	distance target-array (cm)							
(keV)	23.5	18.5	15.5	13.5	11.5	8.5	3.5	
500 keV	8.4	10.2	11.7	12.2	13.1	13.7	13.2	(%)
	3.2	3.9	4.5	4.8	5.3	6.2	7.6	(keV)
1 MeV	6.8	8.4	9.4	10.0	10.7	11.0	10.7	(%)
	5.1	6.3	7.3	8.1	8.7	10.4	12.4	(keV)
1.5 MeV	5.5	6.9	7.9	8.6	9.0	9.5	9.4	(%)
	7.1	9.0	10.2	11.4	12.1	14.3	17.1	(keV)
2 MeV	4.7	6.0	6.9	7.3	8.0	8.4	8.1	(%)
	9.1	11.5	13.1	14.4	15.6	17.8	21.4	(keV)
2.5 MeV	4.1	5.2	5.9	6.4	6.9	7.3	7.1	(%)
	11.3	14.0	16.0	17.5	18.9	22.0	26.2	(keV)
3 MeV	3.6	4.5	5.4	5.6	6.1	6.6	6.5	(%)
	13.1	16.9	19.2	20.4	22.1	25.0	30.5	(keV)
3.5 MeV	3.2	4.0	4.7	5.2	5.2	5.8	5.6	(%)
	14.8	19.2	21.6	24.1	26.4	29.7	34.6	(keV)
4 MeV	3.2	4.1	4.8	5.2	5.6	6.0	6.0	(%)
	19.6	24.6	28.5	31.1	35.0	38.9	44.7	(keV)

7.3 5 double

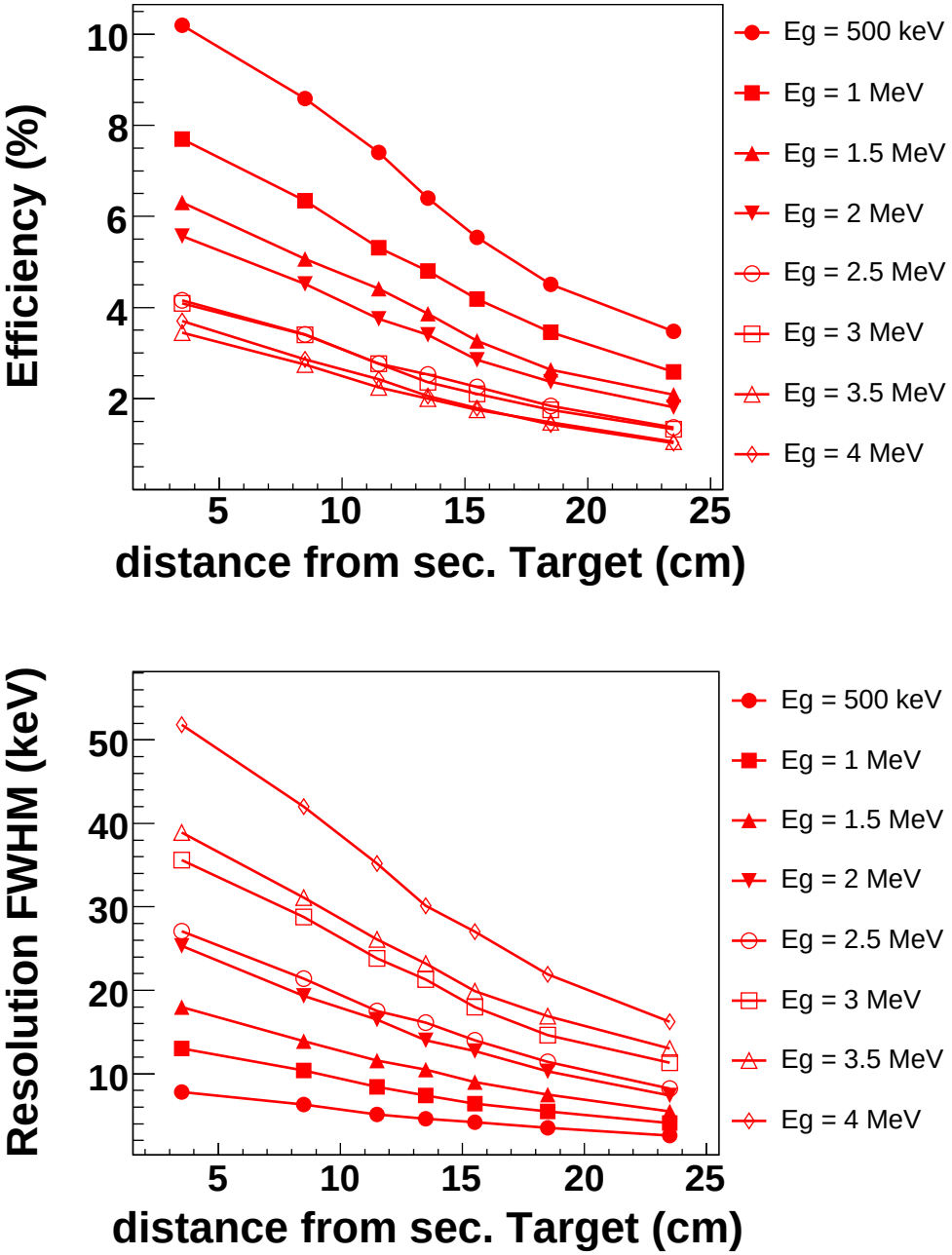

Figure 11: Photopeak efficiency (top) and resolution (bottom) for 5 double AGATA cluster detectors. Each curve corresponds to one gamma-ray energy (see figure label).

Table 4: 5 double AGATA configuration, efficiency and resolution values as a function of the γ-ray energy at rest $E_{\gamma,\circ}$ and $\beta = 0.43$. For each configuration, the first raw are the efficiency values and the second raw the resolution in FWHM.

$E_{\gamma,\circ}$	distance target-array (cm)							
(keV)	23.5	18.5	15.5	13.5	11.5	8.5	3.5	
500 keV	3.5	4.5	5.5	6.4	7.4	8.6	10.2	(%)
	2.6	3.5	4.2	4.6	5.1	6.3	7.8	(keV)
1 MeV	2.6	3.5	4.2	4.8	5.3	6.3	7.7	(%)
	4.1	5.5	6.4	7.4	8.4	10.4	13.0	(keV)
1.5 MeV	2.1	2.6	3.3	3.9	4.4	5.1	6.3	(%)
	5.5	7.5	9.0	10.5	11.6	13.9	18.0	(keV)
2 MeV	1.8	2.4	2.8	3.4	3.8	4.5	5.6	(%)
	7.4	10.3	12.7	14.0	16.5	19.3	25.3	(keV)
2.5 MeV	1.4	1.8	2.2	2.5	2.8	3.4	4.2	(%)
	8.2	11.4	14.0	16.1	17.5	21.4	27.1	(keV)
3 MeV	1.3	1.8	2.1	2.4	2.8	3.4	4.1	(%)
	11.3	14.6	18.0	21.3	23.8	28.8	35.6	(keV)
3.5 MeV	1.0	1.5	1.8	2.0	2.2	2.8	3.5	(%)
	13.0	16.9	19.9	23.2	26.1	31.1	38.9	(keV)
4 MeV	1.0	1.4	1.8	2.1	2.4	2.9	3.7	(%)
	16.2	21.9	27.0	30.1	35.2	42.0	51.8	(keV)

8 Lifetime determination via Doppler Shift Attenuation Method (DSAM)

At forward angles, $\theta_\gamma < 25^\circ - 30^\circ$, the shape of the measured gamma-line reflects mostly the β-value of the recoil fragment at the deexcitation time. Fig. 13 shows this effect, which is reflected in the measured line-shape for the first 2^+ state at 1024 keV in ^{74}Ni, with an expected lifetime of $\tau \sim$1 ps (see Fig. 12). In the latter figures, the three spectra in each panel correspond to variations of this lifetime within a 50% range, i.e. from 0.5 ps to 1.5 ps. The MC-code used as event generator for this application was the one from Ref. [5] with little modifications to interface it with the standard AGATA-code [3]. Basically one can observe two contributions to the shape of the line, a narrow one which arises from decays after (outside) the secondary target, and a broad component arising from decays within the target thickness. In this case, the common secondary beam energy of 100 MeV/u seems to lead to a very broad spread of the in-target component. Therefore, a larger beam energy of 150 MeV/u (Fig. 12 right) seems more favorable because it compresses the in-target component within a narrower energy range.

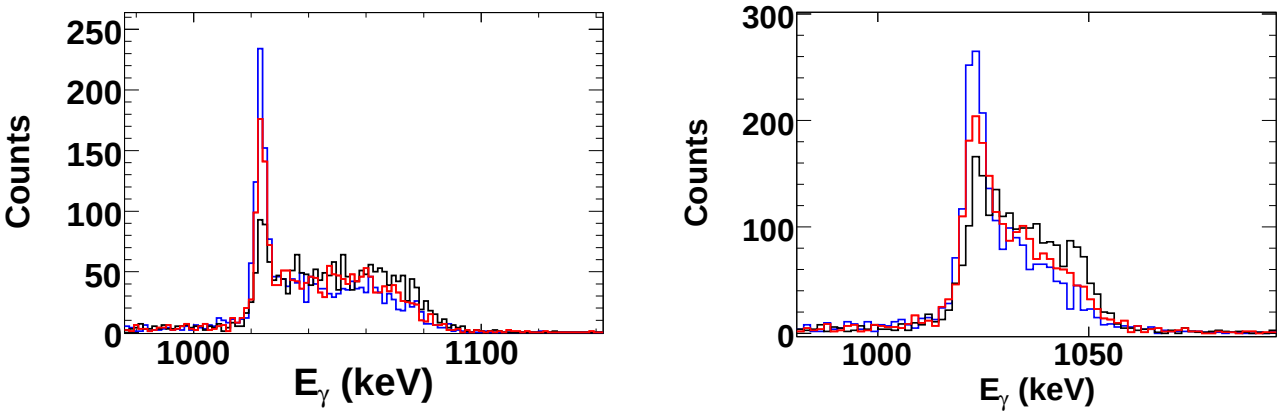

Figure 12: Effect of the deexcitation lifetime on the line-shape measured with AGATA for an angular cut of θ_γ =25°. The left figure corresponds to a secondary beam energy of 100 MeV/u, the right one to 150 MeV/u.

The effect of the lifetime on the line-shape is much less prominent when a Beryllium target is used. This is shown in Fig. 13, where the value of β at the de-excitation time is plotted. This pattern is the main signature in the shape of the measured gamma-line at forward angles. The top panels show a simulation for a 500 mg/cm^2 Be target, at 100 MeV/u (left) and 150 MeV/u (right). In the bottom panels, the same simulation is represented for a 500 mg/cm^2 iron target.

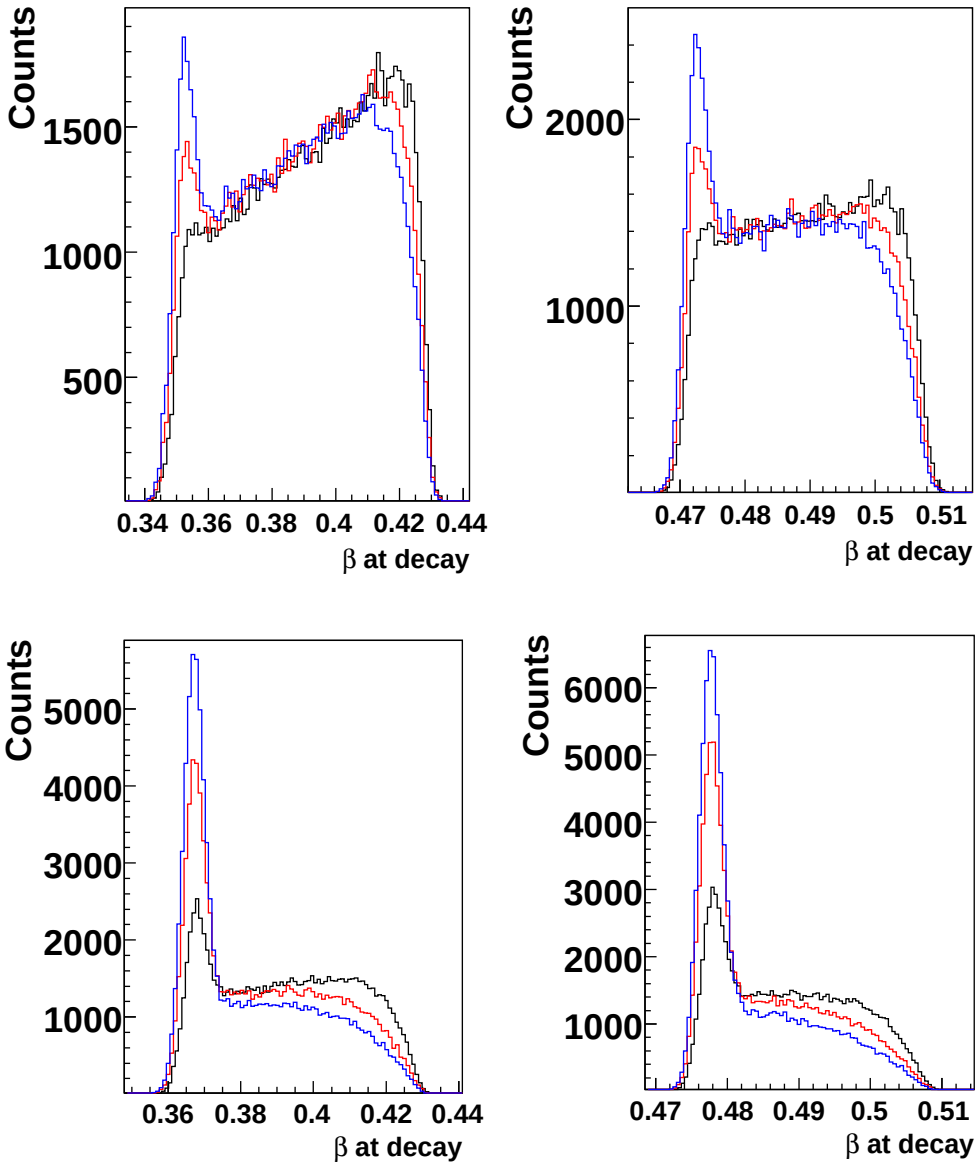

Figure 13: β-value at de-excitation time of the recoil fragment in a Be-target (top) and in Fe-target (bottom), both of them 500 mg/cm^2 thick. The left panels correspond to 100 MeV/u and the right-hand side panels to 150 MeV/u. The three lines in each spectrum are for lifetime values of 0.5 ps, 1 ps and 1.5 ps.

9 Summary and conclusions

At the nominal AGATA target-array distance of 23 cm at least 5 double and 5 triple AGATA clusters are required in order to achieve a γ-ray detection efficiency of $\sim$7% at $E_\gamma = 1$ MeV and $\beta = 0.43$. If a resolution of $\sim$13 keV is permitted, then the same efficiency can be reached for a distance of 11.5 cm using only 5 double and 2 triple cluster detectors.

For target-array distances of 23 cm to 8 cm, the angular range between $\theta_\gamma = 20°$ and $\theta_\gamma = 90°$ can be covered with efficiencies larger than 1% and for an AGATA configuration of 10 triple and 5 double cluster detectors. When target-array distances larger than 23 cm are technically feasible, smaller angles of $\theta_\gamma = 10°$ can be also covered.

Lifetime measurements via the line-shape effect require of dedicated and detailed MC-simulations in order to study the feasibility of the measurement and to optimize the apparatus. In particular, lifetimes of 0.5-1.5 ps seem measurable by using a 500 mg/cm^2 iron target and a secondary beam energy of 150 MeV/u.

References

[1] H. Geissel, P. Armbruster, K. H. Behr, A. Brünle, K. Burkard, M. Chen, H. Folger, B. Franczak, H. Keller, O. Klepper, B. Langenbeck, F. Nickel, E. Pfeng, M. Pfützner, E. Roeckl, K. Rykaczewski, I. Schall, D. Schardt, C. Scheidenberger, K.-H. Schmidt, A. Schröter, T. Schwab, K. Sümmerer, M. Weber, G. Münzenberg, T. Brohm, H.-G. Clerc, M. Fauerbach, J.-J. Gaimard, A. Grewe, E. Hanelt, B. Knödler, M. Steiner, B. Voss, J. Weckenmann, C. Ziegler, A. Magel, H. Wollnik, J. P. Dufour, Y. Fujita, D. J. Vieira, and B. Sherrill. The GSI projectile fragment separator (FRS): a versatile magnetic system for relativistic heavy ions. *Nuclear Instruments and Methods in Physics Research B*, 70:286–297, August 1992.

[2] H. J. Wollersheim, D. E. Appelbe, A. Banu, R. Bassini, T. Beck, F. Becker, P. Bednarczyk, K.-H. Behr, M. A. Bentley, G. Benzoni, C. Boiano, U. Bonnes, A. Bracco, S. Brambilla, A. Brunle, A. Burger, K. Burkard, P. A. Butler, F. Camera, D. Curien, J. Devin, P. Doornenbal, C. Fahlander, K. Fayz, H. Geissel, J. Gerl, M. Gorska, H. Grawe, J. Grebosz, R. Griffiths, G. Hammond, M. Hellstrom, J. Hoffmann, H. Hubel, J. Jolie, J. V. Kalben, M. Kmiecik, I. Kojouharov, R. Kulessa, N. Kurz, I. Lazarus, J. Li, J. Leske, R. Lozeva, A. Maj, S. Mandal, W. Meczynski, B. Million, G. Munzenberg, S. Muralithar, M. Mutterer, P. J. Nolan, G. Neyens, J. Nyberg, W. Prokopowicz, V. F. E. Pucknell, P. Reiter, D. Rudolph, N. Saito, T. R. Saito, D. Seddon, H. Schaffner, J. Simpson, K.-H. Speidel,

J. Styczen, K. Summerer, N. Warr, H. Weick, C. Wheldon, O. Wieland, M. Winkler, and M. Zieblinski. Rare ISotopes INvestigation at GSI (RISING) using gamma-ray spectroscopy at relativistic energies. *Nuclear Instruments and Methods in Physics Research A*, 537:637–657, February 2005.

[3] The Agata Collaboration, E. Farnea, F. Recchia, D. Bazzacco, T. Kröll, Z. Podolyák, B. Quintana, A. Gadea, and The AGATA Collaboration. Conceptual design and Monte Carlo simulations of the AGATA array. *Nuclear Instruments and Methods in Physics Research A*, 621:331–343, September 2010.

[4] D. Bazzacco. mgt code developed within the tmr program 'gamma-ray tracking detectors'.

[5] P. Doornenbal, P. Reiter, H. Grawe, T. Saito, A. Al-Khatib, A. Banu, T. Beck, F. Becker, P. Bednarczyk, G. Benzoni, A. Bracco, A. Bürger, L. Caceres, F. Camera, S. Chmel, F. C. L. Crespi, H. Geissel, J. Gerl, M. Górska, J. GreBosz, H. Hübel, M. Kavatsyuk, O. Kavatsyuk, M. Kmiecik, I. Kojouharov, N. Kurz, R. Lozeva, A. Maj, S. Mandal, W. Meczynski, B. Million, Z. Podolyák, A. Richard, N. Saito, H. Schaffner, M. Seidlitz, T. Striepling, J. Walker, N. Warr, H. Weick, O. Wieland, M. Winkler, and H. J. Wollersheim. Lifetime effects for high-resolution gamma-ray spectroscopy at relativistic energies and their implications for the RISING spectrometer. *Nuclear Instruments and Methods in Physics Research A*, 613:218–225, February 2010.